

# CHEM 26700 (Experimental Physical Chemistry) Lab Reports

Steven Labalme

February 28, 2023

## **Contents**

<b>1</b>	<b>UV-VIS ANALYSIS OF IODINE</b>	<b>1</b>
<b>2</b>	<b>TITLE</b>	<b>5</b>
<b>3</b>	<b>UV-VIS ANALYSIS OF IODINE</b>	<b>10</b>
<b>4</b>	<b>NMR ANALYSIS OF HEXYLAMINE</b>	<b>19</b>
<b>5</b>	<b>GCMS ANALYSIS OF BENZENE IN GASOLINE</b>	<b>25</b>

## List of Figures

1	The absorption spectrum of gaseous I <sub>2</sub> between $\lambda = 5000 - 6500 \text{ \AA}$ . . . . .	1
2	Birge-Sponer plot for the B state. . . . .	3
3	Morse potential curves. . . . .	3
1	Infrared absorption spectrum of air (background spectrum). . . . .	5
2	The five primary vibrational bands in a sample of air. . . . .	5
3	Rovibrational absorption spectrum of HCl. . . . .	6
4	Fitting data on the rovibrational transition wavenumbers $\bar{\nu}$ of HCl vs. a parameter $m$ related to the rotational energy level from which such a rovibrational transition begins. . . . .	7
5	Morse potential curve. . . . .	8
1	The absorption spectrum of gaseous I <sub>2</sub> between $\lambda = 5000 - 6500 \text{ \AA}$ . . . . .	12
2	Birge-Sponer plot for the B state. . . . .	14
3	Morse potential curves. . . . .	15
4	The absorption spectrum (in terms of the directly proportional molar extinction coefficient) of gaseous <sup>5</sup> (blue) and chloroform-based (orange) I <sub>2</sub> between $\lambda = 300 - 800 \text{ nm}$ . . . . .	16
1	<sup>1</sup> H NMR spectrum of hexylamine. The protons on nitrogen exchange rapidly in solution, so since chemical exchanges cause spin decoupling, the A peak is a singlet. . . . .	19
2	<sup>13</sup> C NMR spectrum of hexylamine. Notice that carbon 1 is the most downshifted because it's closest to the electronegative nitrogen atom. . . . .	20
3	A selection of inversion recovery <sup>13</sup> C NMR spectra for different delay times $\tau$ . . . . .	21
4	Determining the spin-lattice relaxation time $T_1$ and the magnetization $M_0$ at equilibrium via nonlinear regression. . . . .	22
5	Two-dimensional <sup>1</sup> H- <sup>13</sup> C HSQC spectrum of hexylamine. . . . .	23
1	Total ion chromatogram of diluted 87-gasoline in pentane. . . . .	25
2	Extracted ion chromatograms and extracted mass spectra for benzene and toluene. . . . .	26
3	Standard addition of benzene. . . . .	27
4	Extracted ion chromatogram of ethylbenzene. . . . .	28
5	Extracted mass spectra of ethylbenzene. . . . .	28
6	Extracted ion chromatogram of mesitylene. . . . .	29
7	Extracted mass spectra of mesitylene. . . . .	29

## List of Tables

1	Peaks and their corresponding transitions. . . . .	2
2	Calculated spectroscopic constants and their reported values. . . . .	3
1	Infrared-active vibrational modes in air molecules. . . . .	6
2	Calculated spectroscopic constants and their reported values. . . . .	7
3	Calculated energy constants and their reported values. . . . .	8
1	Peaks and their corresponding transitions. . . . .	13
2	Calculated spectroscopic constants and their reported values. . . . .	14
1	Standard errors for the above nonlinear regressions. . . . .	22
2	The spin-lattice relaxation time and correlation time for each carbon in hexylamine. . . . .	23
1	Concentration of benzene in gasoline. . . . .	27
2	Concentrations of additional aromatic molecules. . . . .	30

Steven Labalme  
12 January 2023

26 January 2023

## 1 UV-VIS ANALYSIS OF IODINE

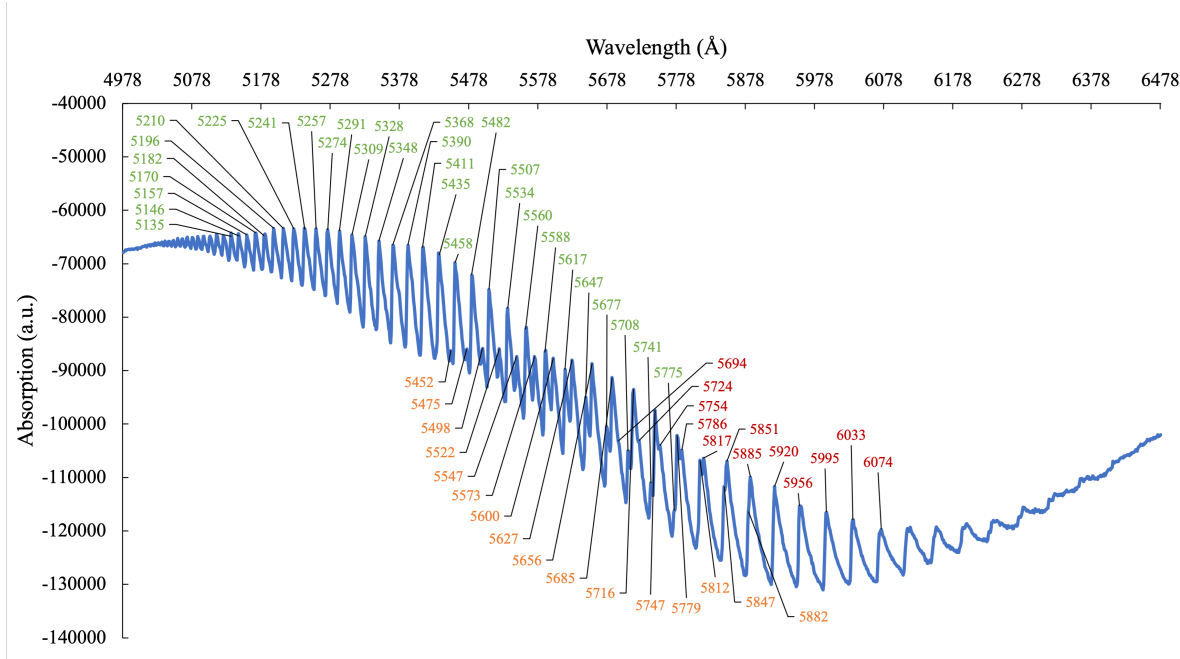


Figure 1: The absorption spectrum of gaseous I<sub>2</sub> between  $\lambda = 5000 - 6500 \text{ \AA}$ .

$v'$	$v''$	$\omega$ (cm $^{-1}$ )	$v'$	$v''$	$\omega$ (cm $^{-1}$ )	$v'$	$v''$	$\omega$ (cm $^{-1}$ )
						10	2	16463
						11	2	16575
						12	2	16680
		13	1	17001		13	2	16789
14	0	17316	14	1	17102	14	2	16891
15	0	17418	15	1	17205	15	2	16992
16	0	17519	16	1	17304	16	2	17091
17	0	17614	17	1	17400	17	2	17190
18	0	17708	18	1	17494	18	2	17283
19	0	17803	19	1	17590	19	2	17379
20	0	17895	20	1	17680	20	2	17470
21	0	17985	21	1	17771	21	2	17562
22	0	18070	22	1	17857			
23	0	18158	23	1	17943			
24	0	18241	24	1	18027			
25	0	18321	25	1	18109			
26	0	18399	26	1	18188			
27	0	18480	27	1	18264			
28	0	18552	28	1	18341			
29	0	18628						
30	0	18698						
31	0	18768						
32	0	18835						
33	0	18900						
34	0	18960						
35	0	19022						
36	0	19080						
37	0	19138						
38	0	19193						
39	0	19245						
40	0	19297						
41	0	19342						
42	0	19391						
43	0	19432						
44	0	19474						

Table 1: Peaks and their corresponding transitions.

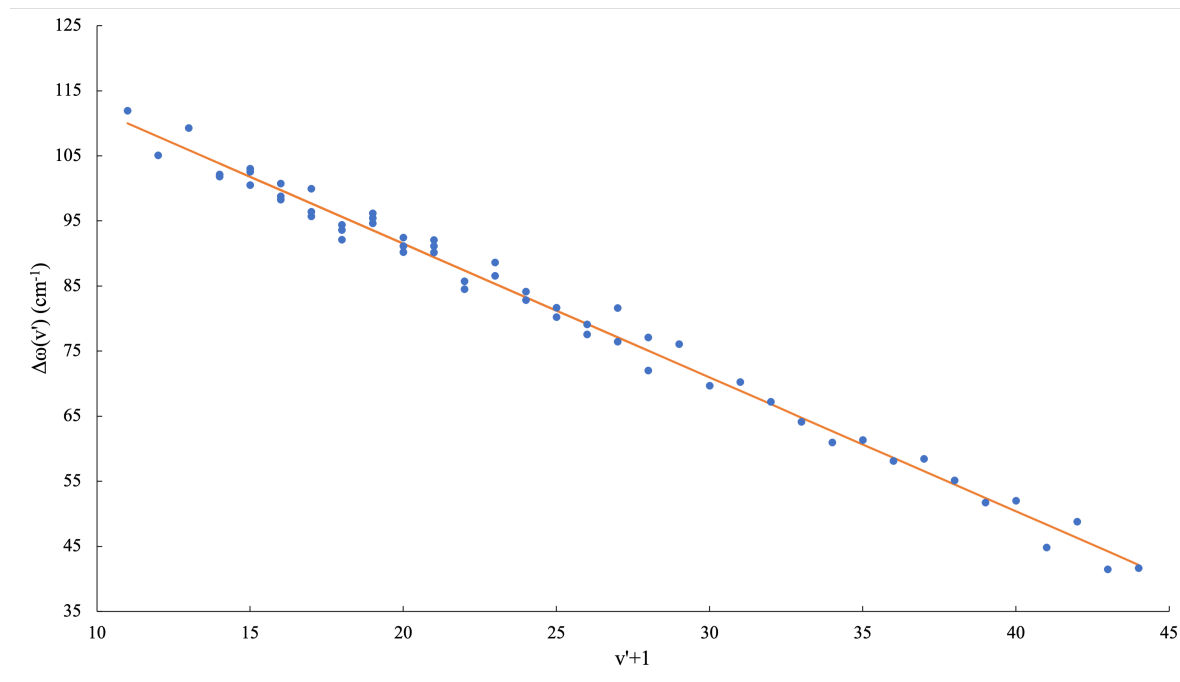


Figure 2: Birge-Sponer plot for the B state.

	$\bar{\nu}'_e$	$\bar{\nu}'_e x'_e$	$D'_e$	$D'_0$	$\bar{\nu}''_e$	$\bar{\nu}''_e x''_e$	$D''_e$	$D''_0$	$T_e$
<b>Calculated values</b>	132.62	1.0279	4277.2	4211.1	216.10	1.2583	9278.5	9170.7	12604
<b>Literature values<sup>1,2</sup></b>	125.69	0.764	4112	4046	214.50	0.614	12244	12137	15769.01

Table 2: Calculated spectroscopic constants and their reported values.

Note that the units for all values in Table 2 is  $\text{cm}^{-1}$ .

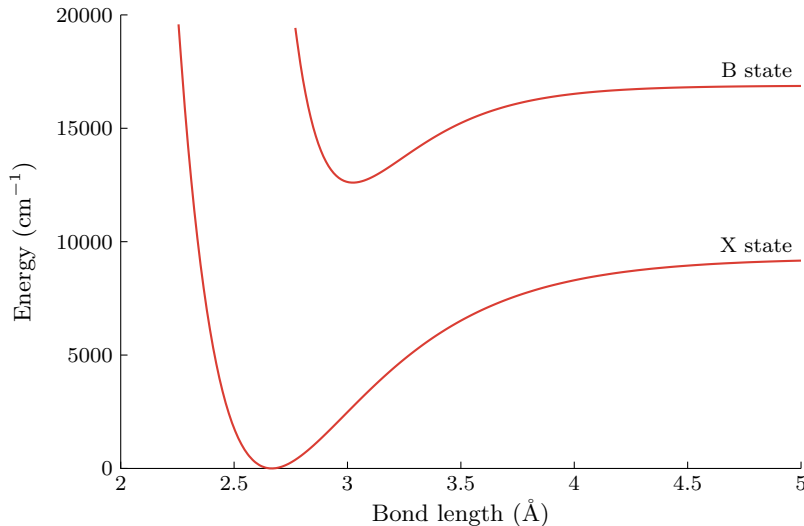


Figure 3: Morse potential curves.

## References

- (1) Huber, K. P.; Herzberg, G. H. In *NIST Chemistry WebBook, NIST Standard Reference Database Number 69*, Linstrom, P. J., Mallard, W. G., Eds., <https://doi.org/10.18434/T4D303>; National Institute of Standards and Technology: Gaithersburg MD, 20899; Chapter Constants of Diatomic Molecules.
- (2) McNaught, I. J. The Electronic Spectrum of Iodine Revisited. *J. Chem. Educ.* **1980**, *57*, 101–105.
- (3) Lant, H. Electronic Spectroscopy: Absorption Spectra of Molecular Iodine in the Gas Phase, Rev. 1-21-23, 2023.
- (4) Verma, R. D. Ultraviolet Resonance Spectrum of the Iodine Molecule. *J. Chem. Phys.* **1960**, *32*, 738–749.
- (5) Saiz-Lopez, A.; Saunders, R. W.; Joseph, D. M.; Ashworth, S. H.; Plane, J. M. C. Absolute absorption cross-section and photolysis rate of I<sub>2</sub>. *Atmos. Chem. Phys.* **2004**, *4*, 1443–1450.

Steven Labalme  
26 January 2023

2 February 2023

## 2 TITLE

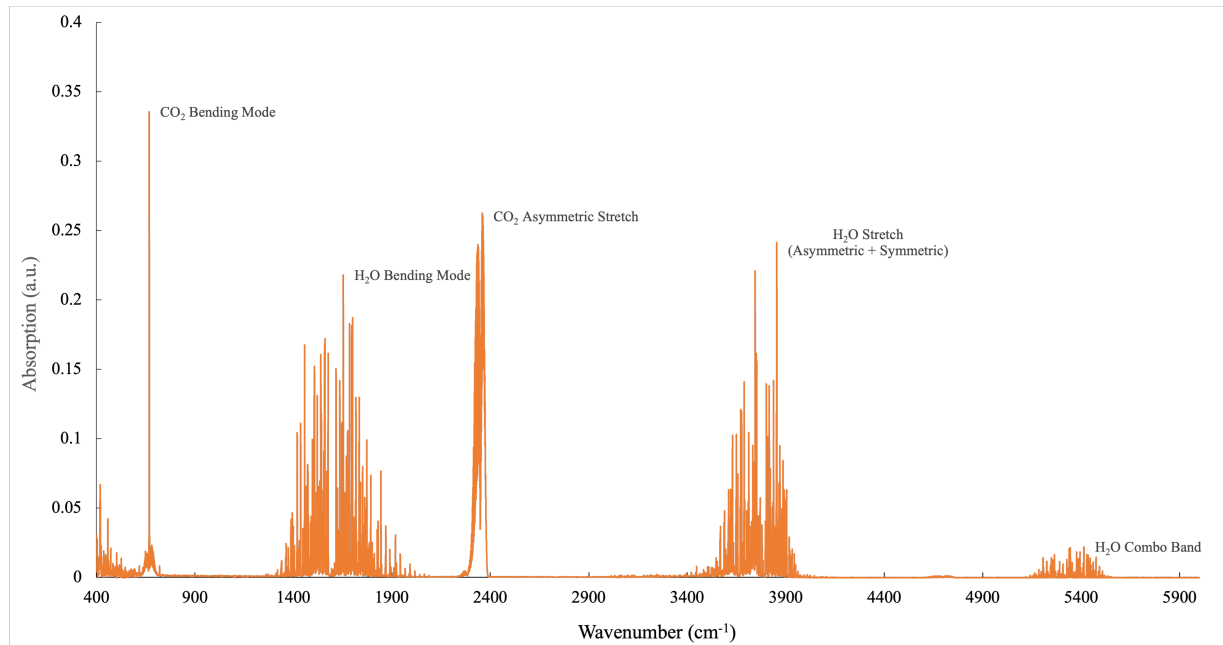


Figure 1: Infrared absorption spectrum of air (background spectrum).

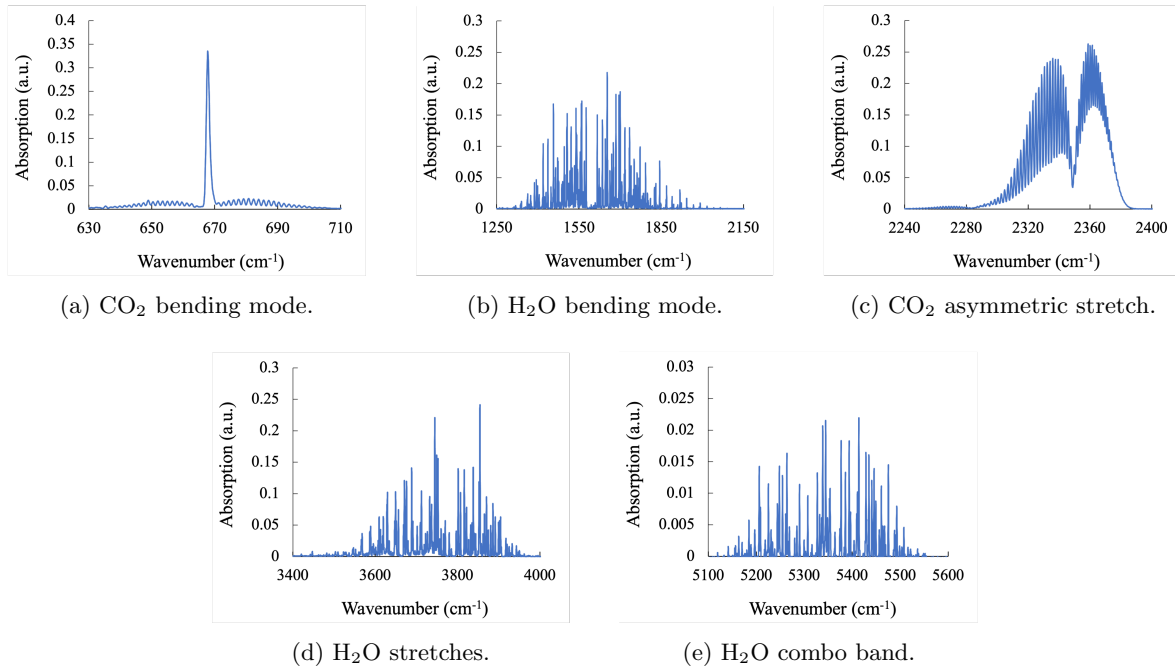


Figure 2: The five primary vibrational bands in a sample of air.

Wavenumber Range ( $\text{cm}^{-1}$ )	Molecule	Vibrational Band
630-710	$\text{CO}_2$	Bending
1250-2150	$\text{H}_2\text{O}$	Bending
2240-2400	$\text{CO}_2$	Asymmetric stretch
3400-4000	$\text{H}_2\text{O}$	Asymmetric & symmetric stretch
5100-5600	$\text{H}_2\text{O}$	Combo band

Table 1: Infrared-active vibrational modes in air molecules.

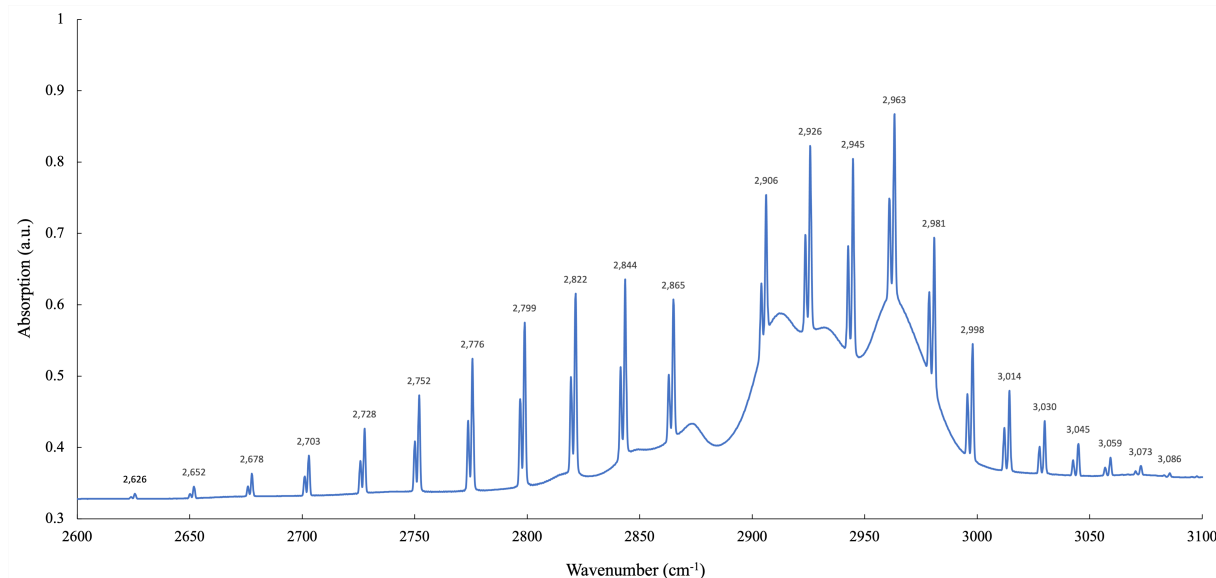


Figure 3: Rovibrational absorption spectrum of HCl.

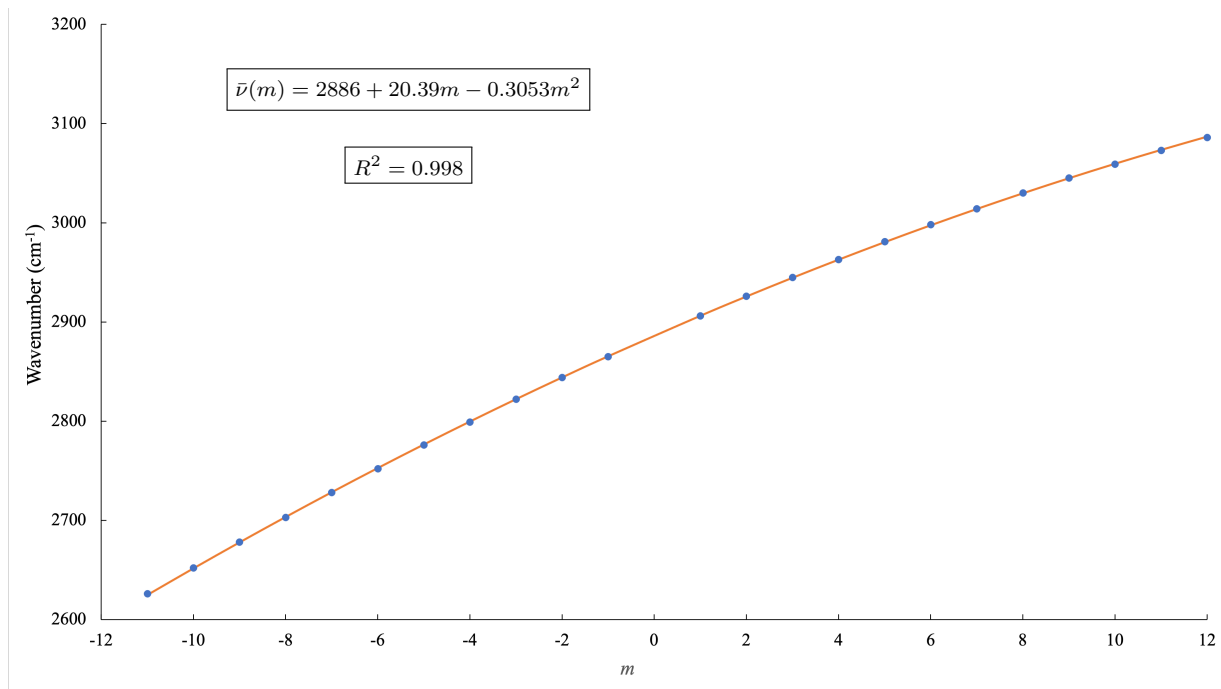


Figure 4: Fitting data on the rovibrational transition wavenumbers  $\bar{\nu}$  of HCl vs. a parameter  $m$  related to the rotational energy level from which such a rovibrational transition begins.

	$B_e$ (cm <sup>-1</sup> )	$\alpha_e$ (cm <sup>-1</sup> )	$\bar{\nu}_0$ (cm <sup>-1</sup> )
<b>Calculated values</b>	10.50	0.3053	2886
<b>Literature values</b>	10.59 <sup>1</sup>	0.3072 <sup>1</sup>	2991 <sup>1</sup>

Table 2: Calculated spectroscopic constants and their reported values.

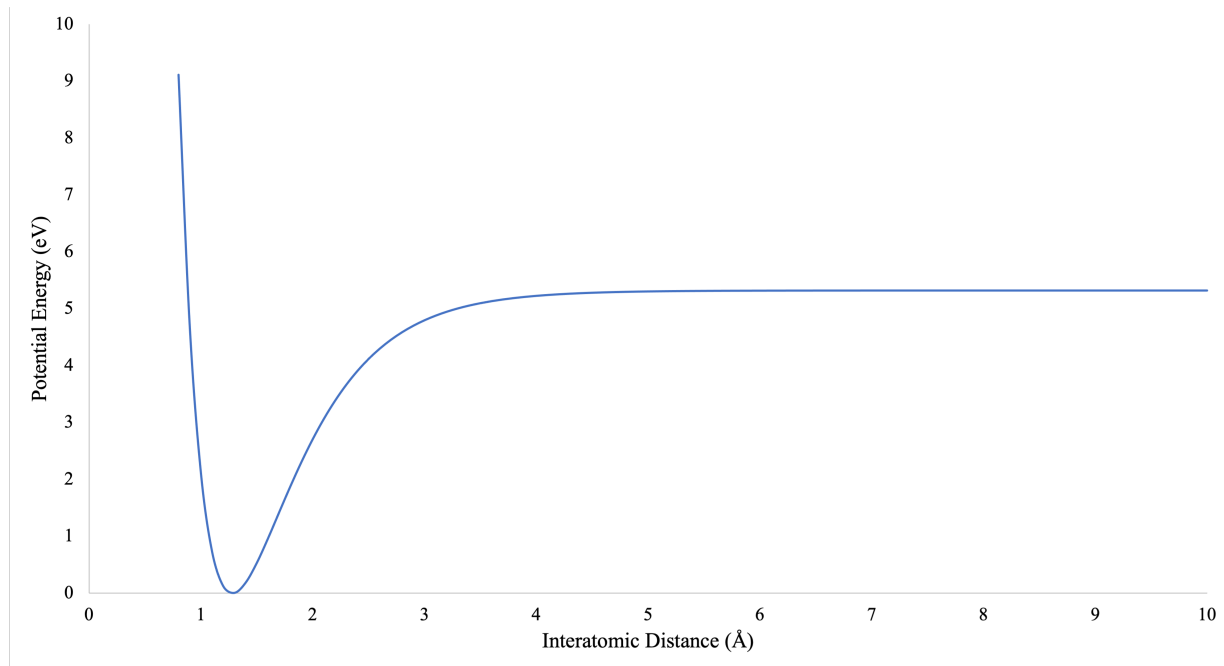


Figure 5: Morse potential curve.

	$\bar{\nu}_e$ ( $\text{cm}^{-1}$ )	$x_e$	$D_e$ (eV)	$r_e$ ( $\text{\AA}$ )
<b>Calculated values</b>	2990	0.01741	5.320	1.281
<b>Literature values</b>	2991 <sup>1</sup>	0.01766 <sup>1</sup>	5.319 <sup>1</sup>	1.275 <sup>1</sup>

Table 3: Calculated energy constants and their reported values.

## References

- (1) Huber, K. P.; Herzberg, G. H. In *NIST Chemistry WebBook, NIST Standard Reference Database Number 69*, Linstrom, P. J., Mallard, W. G., Eds., <https://doi.org/10.18434/T4D303>; National Institute of Standards and Technology: Gaithersburg MD, 20899; Chapter Constants of Diatomic Molecules.
- (2) McNaught, I. J. The Electronic Spectrum of Iodine Revisited. *J. Chem. Educ.* **1980**, *57*, 101–105.
- (3) Lant, H. Electronic Spectroscopy: Absorption Spectra of Molecular Iodine in the Gas Phase, Rev. 1-21-23, 2023.
- (4) Verma, R. D. Ultraviolet Resonance Spectrum of the Iodine Molecule. *J. Chem. Phys.* **1960**, *32*, 738–749.
- (5) Saiz-Lopez, A.; Saunders, R. W.; Joseph, D. M.; Ashworth, S. H.; Plane, J. M. C. Absolute absorption cross-section and photolysis rate of I<sub>2</sub>. *Atmos. Chem. Phys.* **2004**, *4*, 1443–1450.

Steven Labalme  
TA: Rowan Simonet  
Lab partners: Eric Yuan and Kate Kaplin  
12 January 2023

10 February 2023

### 3 UV-VIS ANALYSIS OF IODINE

#### Abstract

The goal of this experiment is to determine several spectroscopic constants of iodine and use them to calculate the potential energy surface, approximated as a Morse potential, of the ground and second excited states. Additionally, it is desired to compare solution-phase and gas-phase data to obtain insight into how phase changes alter molecular dynamics.

As a result of both gas- and solution-phase analyses, the fundamental vibrational frequency, first anharmonicity constant, well depth, dissociation energy (from the zero point energy), difference in energy between the X and B states, and Morse constant  $\beta$  were calculated.

The aim is to provide an experimental verification of the basic quantum mechanical theory of molecular transition mechanics.

#### Introduction

The experiment described herein has two main parts. The primary purpose of the first of these is to determine several spectroscopic constants of diatomic iodine ( $I_2$ ) from the gas-phase ultraviolet-visible (UV-Vis) absorption spectrum and use them to calculate the potential energy surface, approximated as a Morse potential, of the ground ( $^1\Sigma_g^+$ ) and second excited ( $^3\Pi_{\text{ou}}^+$ ) states<sup>3,2</sup>. The primary purpose of the second of these is obtain a solution-phase UV-Vis absorption spectrum and, from it, calculate the molar extinction coefficient.

From the gas-phase data in particular, we can obtain the frequencies, anharmonicities, and magnitudes of each electronic state, the dissociation energies of each electronic state, and more, but we will only focus on the first two herein<sup>2</sup>. From the solution-phase data, we can only obtain the frequency and magnitude of the transition.

As mentioned above, we will collect our data via UV-Vis spectroscopy (gas phase and solution phase). We will analyze anharmonicity (and its derived constants) using a linear model and hence linear regression. All theoretical calculations build up to the construction of a Morse potential.

The main theoretical idea behind the experiment is that incoming radiation couples to the eigenstates of the system. Specifically, frequencies of radiation that (nearly) exactly match the difference in energy between two quantum states are capable of causing a transition. In the UV-Vis range, this excitation occurs between vibronic energy levels. The electronic energy levels are represented by discrete potential energy surfaces (PES's), and the vibrational energy levels occur as sublevels within the larger electronic levels. If we approximate the electronic potential wells as parabolas (corresponding to a harmonically oscillating molecule), we can prove via quantum mechanics that the energies of the vibrational sublevels depend on an indexing parameter  $v$  via

$$E_v = \bar{\nu}_e \left( v + \frac{1}{2} \right)$$

where  $\bar{\nu}_e$  is the fundamental vibrational frequency. Realizing that a harmonic oscillator is not a good approximation, we can introduce anharmonicity into the math by expanding the above energy levels as a power series in  $v + 1/2$ . Using this energy function to second order, we can derive a formula for the spacing between adjacent vibrational energy levels that is linear. This formula comes in two flavors, one for changes in the vibrational energy level to which an electron is excited and one for changes in the ground state vibrational energy level (i.e., fundamental transitions vs. hot bands). Both are listed below.

$$\Delta\bar{\nu}(v') = \bar{\nu}'_e - 2\bar{\nu}'_e x'_e (v' + 1)$$

$$\Delta\bar{\nu}(v'') = \bar{\nu}''_e - 2\bar{\nu}''_e x''_e (v'' + 1)$$

In the above equations,  $x_e$  is the first anharmonicity constant, and the other variables are as defined above.

Thus, fitting the peaks on a UV-Vis spectrum (which correspond to distinct vibronic transitions) allows us to reverse engineer the fundamental frequency and anharmonicity parameters. These parameters give information on the shape of the potential well that can be fit to a Morse potential via<sup>3</sup>

$$D_e \approx \frac{\bar{\nu}_e}{4x_e} \quad \beta = \bar{\nu}_e \pi \cdot \sqrt{\frac{2c\mu}{hD_e}}$$

In the above equations,  $c = 2.998 \times 10^8 \text{ m s}^{-1}$  is the speed of light,  $\mu = 1.06 \times 10^{-25} \text{ kg}$  is the reduced mass of  $\text{I}_2$ ,  $h = 6.626 \times 10^{-34} \text{ Js}$  is Planck's constant, and all other variables are as defined above.

Per Verma [4], the Morse potential is an excellent approximation for the PES of  $\text{I}_2$ , even among similar diatomics, so we can expect physically comparable results from the following equation even using such a crude experiment and theoretical model.

$$U(r) = D_e(e^{-\beta(r-r_e)} - 1)^2$$

In the above equation,  $U$  is the potential energy,  $r$  is the bond distance on which  $U$  depends,  $\beta$  is the Morse constant,  $r_e$  is the equilibrium constant, and e is Euler's number.

## Experimental

To collect the gas-phase spectrum, an apparatus centered around a SPEX 500M monochromator was used. Said apparatus also included a light source, the  $\text{I}_2$  sample, a light shutter, and an RCA 6217 photomultiplier tube (PMT) which functioned as a detector. Removal of external light was accomplished by carrying out the experiment in a darkened room and shrouding the PMT in an additional blanket. Data collection was performed in LabView from National Instruments<sup>3</sup>. During the post-collection analysis phase, extra care was taken at the lower ends of  $(v', 0)$ ,  $(v', 1)$ , and  $(v', 2)$  peaks since hot bands eventually outweigh other data. However, the hot bands were still analyzed as they actually make it possible to obtain much more data from the excited-state Birge-Sponer plot, and data at all for a ground-state Birge-Sponer plot<sup>2</sup>.

To collect the solution-phase spectrum, an Ocean Optics USB4000 spectrometer was connected to a standard desktop computer running OceanView. The solvent used for  $\text{I}_2$  was chloroform ( $\text{CHCl}_3$ ). An extremely dilute sample was used to bring the data in to the Beer's Law region (to allow for calculation of the molar extinction coefficient, as previously mentioned). Beer's law is given by

$$A = \varepsilon bC$$

where  $A$  is absorbance,  $\varepsilon$  is the molar extinction coefficient,  $b$  is the path length (1 cm in this case since that's the width of the cuvette), and  $C$  is the concentration of the dilution ( $2.8 \times 10^{-4} \text{ M}$  in this case).

The overall procedure was as follows. First, a broad-spectrum scan of the gas-phase sample was collected to identify the region of interest. Next, a narrow-range spectrum was collected to far greater accuracy, allowing for the resolution of vibrational transitions. A subsequent calibration step (using a mercury lamp that emits at one known characteristic wavelength) was performed to account for any error in the monochromator. For the solution, a chloroform and cuvette background, and a dark background were taken. Then, the sample was diluted using 0.7 mL of a 0.01 M stock solution and an additional 24.3 mL of pure chloroform; the result was a  $2.8 \times 10^{-4} \text{ M}$  solution of  $\text{I}_2$  in  $\text{CHCl}_3$ . Lastly, a UV-Vis absorption spectrum of this sample was taken.

Safety goggles and nitrile gloves were used at all times when handling chloroform-containing samples.

## Results

As determined by the initial broad-spectrum scan, the gas-phase spectrum was collected between 5000-6500 Å. It is plotted below in Figure 1. Note that the colored numbers correspond to the wavelengths of certain vibrational transitions (green for ground state, orange for the first hot band, red for the second hot band).

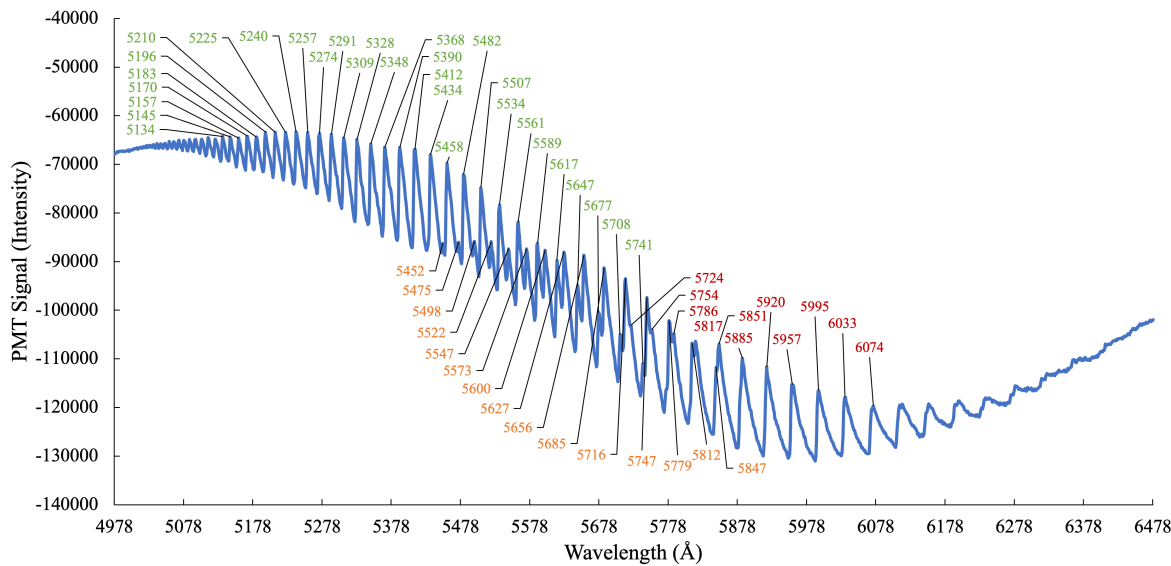


Figure 1: The absorption spectrum of gaseous  $\text{I}_2$  between  $\lambda = 5000 - 6500 \text{ \AA}$ .

Since the PMT is not capable of measuring absorption directly and unforeseen circumstances prevented the collection of a background spectrum in a timely manner, the spectrum is plotted in *intensity* vs. wavelength instead of the standard *absorption* vs. wavelength. Support for an accurate measurement of the wavelength comes from the aforementioned mercury lamp calibration step, and steps have been taken to ensure that the PMT intensity (as described above) is also accurate.

The overall trend observed in Figure 1 is representative of the electronic absorption band, while the fine structure is vibrational in nature. The variable peak spacing is representative of anharmonicity and is characterized below in Figure 2.

First, though, the peaks labeled in Figure 1 are tabulated and assigned to vibronic transitions using known reference values. The result is as follows. Note that wavelength has been converted to wavenumber.

$v'$	$v''$	$\omega$ (cm $^{-1}$ )	$v'$	$v''$	$\omega$ (cm $^{-1}$ )	$v'$	$v''$	$\omega$ (cm $^{-1}$ )
						10	2	16464
						11	2	16576
						12	2	16681
						13	2	16787
			14	1	17103	14	2	16892
15	0	17419	15	1	17206	15	2	16992
16	0	17519	16	1	17304	16	2	17091
17	0	17615	17	1	17400	17	2	17191
18	0	17709	18	1	17495	18	2	17283
19	0	17803	19	1	17590	19	2	17379
20	0	17892	20	1	17680	20	2	17470
21	0	17982	21	1	17771			
22	0	18070	22	1	17857			
23	0	18159	23	1	17944			
24	0	18242	24	1	18028			
25	0	18322	25	1	18109			
26	0	18402	26	1	18188			
27	0	18477	27	1	18265			
28	0	18553	28	1	18342			
29	0	18629						
30	0	18699						
31	0	18769						
32	0	18836						
33	0	18900						
34	0	18961						
35	0	19022						
36	0	19084						
37	0	19139						
38	0	19194						
39	0	19246						
40	0	19294						
41	0	19342						
42	0	19391						
43	0	19436						
44	0	19478						

Table 1: Peaks and their corresponding transitions.

Using the data in Table 1 and the  $\Delta\bar{\nu}(v')$  equation from the introduction, it is possible to construct and characterize a Birge-Sponer plot (Figure 2) to determine both the fundamental vibration frequency and the first anharmonicity constant. All three data sets ( $v'' = 0, 1, 2$ ) are plotted on top of each other, and are plotted versus the change in wavenumber.

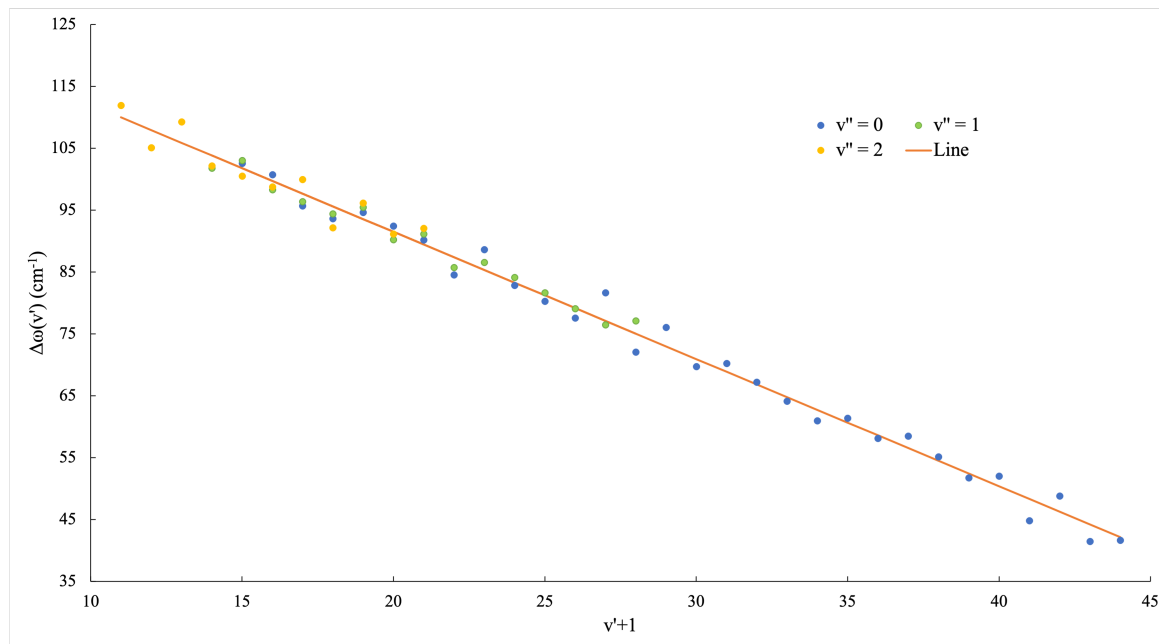


Figure 2: Birge-Sponer plot for the B state.

Evidently, the linear analysis provides a remarkable fit to the data, and it is not immediately obvious that a higher-order energy equation (e.g., cubic, quartic, etc.) would have been necessary to account for additional anharmonicity.

The above analysis was repeated for the  $\Delta\nu(v'')$  data. From  $\bar{\nu}'_e$ ,  $\delta\nu'_e x'_e$ ,  $\bar{\nu}''_e$ , and  $\delta\nu''_e x''_e$ , the ground and excited state dissociation energies from both the bottom of the energy well and the zero point energy can be calculated:  $D'_e$ ,  $D'_0$ ,  $D''_e$ , and  $D''_0$ . The calculation of the energy gap between electronic levels  $T_e$  followed from the previous data and additional information on the hypothetical energy of a dissociated excited I<sub>2</sub> molecule. All constants are summarized below.

	$\bar{\nu}'_e$	$\bar{\nu}'_e x'_e$	$D'_e$	$D'_0$	$\bar{\nu}''_e$	$\bar{\nu}''_e x''_e$	$D''_e$	$D''_0$	$T_e$
Calculated values	132.22	1.019	4288.6	4222.7	214.97	0.912	12672	12564	15 986.11
Literature values	125.69 <sup>1</sup>	0.764 <sup>1</sup>	5169.3	5106.6	214.50 <sup>1</sup>	0.614 <sup>1</sup>	18 734	18 627	15 769.01 <sup>1</sup>

Table 2: Calculated spectroscopic constants and their reported values.

Note that the unit for all values in Table 2 is cm<sup>-1</sup>. Also note that the  $D_e$  and  $D_0$  values were calculated from the NIST  $\bar{\nu}'_e$  and  $x'_e = \bar{\nu}'_e x'_e / \bar{\nu}'_e$  values using Equations 9 and 12 in Lant [3], respectively.

The experimental values in Table 2 may be plugged into two Morse potential equations as follows.  $D_e$  values go in directly.  $\beta$  values must be calculated as in the introduction. Equilibrium bond length values are found in Lant [3]. And  $T_e$  gives the vertical offset between the two equations (the zero of energy was arbitrarily defined to be the bottom of the ground (X) state potential well).

Additionally, as wavenumbers have been used throughout the analysis, they are used as the unit of energy on the y-axis of Figure 3 below. Lastly, angstroms are a natural scale on which to discuss molecules, so bond length (the x-axis below) is given in terms of it. All above determinations of error suggest that the variables are being measured largely accurately.

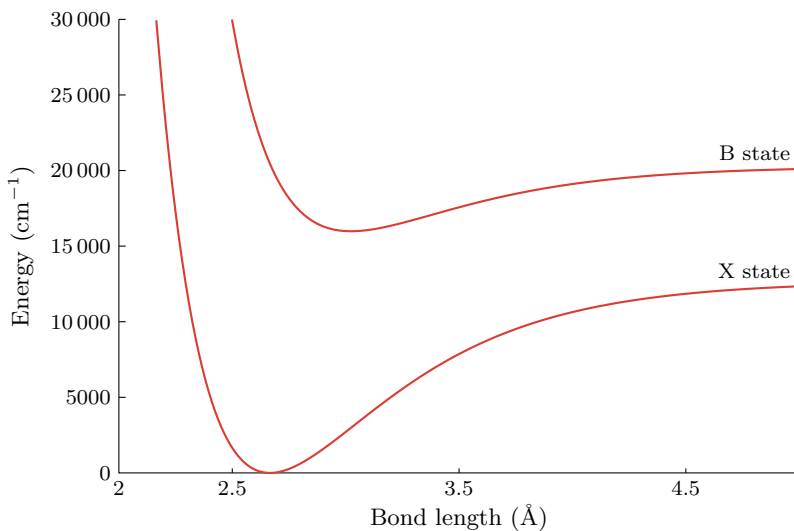


Figure 3: Morse potential curves.

From the above plot, it can be seen that the excited state has a slightly longer average bond length (as is to be expected for a molecule that is vibrating more extremely). Additionally, the ground state energies are generally more concentrated in one area, whereas the excited state ones are more spread out.

Lastly, all of the gas-phase analysis above is compared to the solution phase data. Both the initial data from Figure 1 (or rather a separate data set in terms of the molar extinction coefficient, which is closely related to absorption, obtained from Saiz-Lopez et al. [5]) and the solution-phase data are plotted in Figure 4 on the same set of axes. Expressing the data in terms of molar extinction coefficient is driven by the nature of the data from Saiz-Lopez et al. [5]; data from the solution-phase experiment performed by the authors is readily converted from absorption to molar extinction coefficient using Beer's law (per the introduction). Wavelength has been adjusted for as previously mentioned.

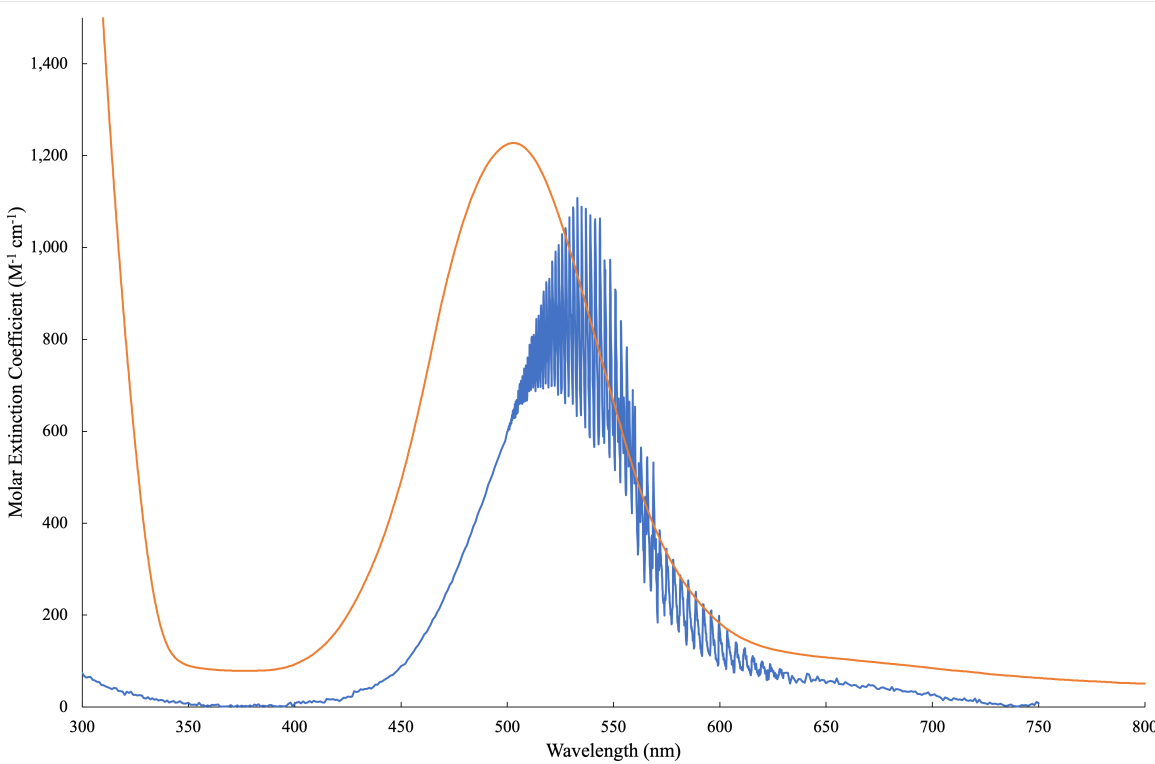


Figure 4: The absorption spectrum (in terms of the directly proportional molar extinction coefficient) of gaseous<sup>5</sup> (blue) and chloroform-based (orange) I<sub>2</sub> between  $\lambda = 300 - 800$  nm.

The maximum of the gas-phase electronic band is  $1089 \text{ M}^{-1} \text{ cm}^{-1}$  and occurs at  $\lambda = 534.9 \text{ nm}$ . The maximum of the solution-phase electronic band is  $1227 \text{ M}^{-1} \text{ cm}^{-1}$  at  $\lambda = 502.7 \text{ nm}$ .

Half the gas-phase electronic maximum is  $544.5 \text{ M}^{-1} \text{ cm}^{-1}$ . The line  $\varepsilon = 544.5 \text{ M}^{-1} \text{ cm}^{-1}$  intersects the left side of the peak at  $\lambda = 496 \text{ nm}$  and the right side between  $\lambda = 548.1 - 565.8 \text{ nm}$ . Taking the average yields

$$\frac{548.1 + 565.8}{2} = 557.0$$

Thus, the full width of the absorption band at half the maximum height (FWHM) is

$$\text{FWHM} = 557.0 - 496 = 61 \text{ nm}$$

Half of the solution-phase electronic maximum is  $613.5 \text{ M}^{-1} \text{ cm}^{-1}$ . The line  $\varepsilon = 613.5 \text{ M}^{-1} \text{ nm}^{-1}$  intersects the left side of the peak at  $\lambda_1 = 456.7 \text{ nm}^{-1}$  and the right side at  $\lambda_2 = 553.19 \text{ nm}^{-1}$ . Therefore, the FWHM is

$$\text{FWHM} = 96.5 \text{ nm}$$

The molar extinction coefficient can be read off the graph above as the electronic maximum, yielding  $1227 \text{ M}^{-1} \text{ cm}^{-1}$ .

## Discussion

Assuming that each vibrational peak corresponds to a Lorentzian lineshape, the “disappearance” of vibrational peaks in the solution phase likely is actually representative of extreme flattening of the peaks. Molecularly, this corresponds to heightened damping of the oscillator, which would make sense in solution as all I<sub>2</sub> molecules will be restricted in motion by the surrounding solvent molecules. Additionally, the electronic blue shift means that more energy in general is required to excite the molecule in solution. One possible factor that could account for the shift in wavelength is that effective wavelength is shortened in substances

(including chloroform) due to their index of refraction. However, this effect is more an empirical one than an actual one (light is just bouncing around more and thus “looks” slower), so this could probably not explain the corresponding energy shift. A better theory is that the ground and excited states actually get farther apart in solution. One potential cause of this is stabilization of the ground state due to solvent effects. This stabilization would not similarly apply to the excited state since by the Born-Oppenheimer approximation, solvent molecules will not have time to rearrange on the timescale of the transition.

For free molecular dynamics, though, it is far more instructive to look at the gas phase. The light excites an electron from its ground electronic state and a ground (or slightly excited) vibrational state to an excited electronic state and a much higher vibrational state in a vibronic transition.

Theory and measured literature values are generally pretty close, and always on the same order of magnitude (sometimes much better). A precise quantitative treatment was not performed, but it can be assumed that this is pretty close, given the crudeness of the setup.

Throughout the experiment, steps were taken to collect baselines and correct for instrumental error. To calibrate the SPEX 500M monochromator, a mercury lamp that emits strongly at one characteristic frequency was used. This known frequency was compared against that recorded by the monochromator and PMT to determine an offset in the values. With the solution-phase setup, both a dark baseline (for system error) and a chloroform/cuvette baseline (for setup error) were subtracted from our final data to hopefully isolate the UV/Vis absorption due to  $I_2$  alone.

However, some error likely remained. For example, the gas-phase spectrum was only measured to 1 Å resolution. The machine was capable of going further, and doing so could have yielded more exact peak assignments. Given that even 1 Å shifts in a few peaks can have a remarkable effect on the ultimate analysis, it is certainly possible that being exact to decimal angstroms could have been helpful. Additionally, the monochromator itself is very old and likely has become less exact with age in ways that even mercury calibration cannot fully account for. The not-super-rigorous exclusion of external light sources could also have lead to error in peak height analysis, perhaps affecting calculations of the electronic band maxima. Possible error could have also come from sublimed iodine on the surface of the tube windows<sup>2</sup>. Human error in the chloroform setup included the fact that the instrument was manually put together and the shield, for instance, could have been in slightly different places each time. Additionally, the dilution was carried out by hand, so there could have been error in the calculation of the concentration of the solution. Moreover, chloroform is very volatile, so subtle concentration changes likely occurred throughout the experiment due to evaporation. On the data-analysis side of things, the Morse potential in and of itself is a crude model. Using the Lennard-Jones potential, for instance, would have been more accurate. Additionally, the anharmonicity was only approximated to first order, not to higher order as it certainly could have been. Thus, the PES's in Figure 3 and data in Table 2 may not even be entirely representative of the data collected.

However, given the remarkable closeness to literature values, the data was likely pretty good with a few of the aforementioned sources of error disproportionately affecting the overall data quality.

## Conclusion

The most important results are that solvent effects blue shift the overall transitions between solution-phase and gas-phase data, and that there is an experimental basis for anharmonicity. From Figure 2, a linear fit is not a bad approximation of anharmonicity, so the Morse potential is at least somewhat justified. Further evidence for this justification comes from Verma [4].

The goal of this experiment was to determine several spectroscopic constants of  $I_2$  and use them to calculate the potential energy surface, approximated as a Morse potential, of the ground and second excited states. This was achieved. Additionally, the researchers sought to compare solution-phase and gas-phase data to obtain insight into how phase changes alter molecular dynamics. This was also achieved.

The result is a verification of the quantum-mechanical theory of light absorption. Additionally, this experiment shows that even simple models like the Morse potential can have real predictive power. Separately, it shows that molecular interaction effects in condensed phases (and the lack thereof in expanded phases) have identifiable optical effects.

## References

- (1) Huber, K. P.; Herzberg, G. H. In *NIST Chemistry WebBook, NIST Standard Reference Database Number 69*, Linstrom, P. J., Mallard, W. G., Eds., <https://doi.org/10.18434/T4D303>; National Institute of Standards and Technology: Gaithersburg MD, 20899; Chapter Constants of Diatomic Molecules.
- (2) McNaught, I. J. The Electronic Spectrum of Iodine Revisited. *J. Chem. Educ.* **1980**, *57*, 101–105.
- (3) Lant, H. Electronic Spectroscopy: Absorption Spectra of Molecular Iodine in the Gas Phase, Rev. 1-21-23, 2023.
- (4) Verma, R. D. Ultraviolet Resonance Spectrum of the Iodine Molecule. *J. Chem. Phys.* **1960**, *32*, 738–749.
- (5) Saiz-Lopez, A.; Saunders, R. W.; Joseph, D. M.; Ashworth, S. H.; Plane, J. M. C. Absolute absorption cross-section and photolysis rate of I<sub>2</sub>. *Atmos. Chem. Phys.* **2004**, *4*, 1443–1450.

Steven Labalme  
2 February 2023

16 February 2023

## 4 NMR ANALYSIS OF HEXYLAMINE

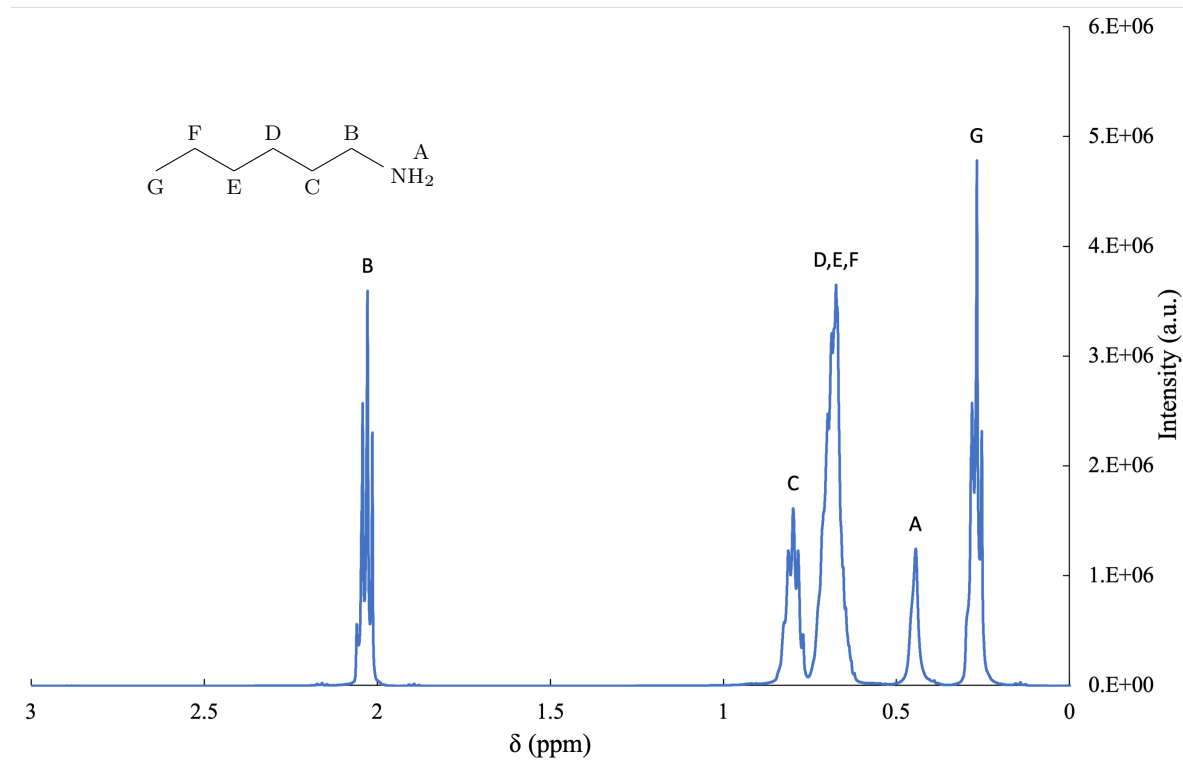


Figure 1:  $^1\text{H}$  NMR spectrum of hexylamine. The protons on nitrogen exchange rapidly in solution, so since chemical exchanges cause spin decoupling, the A peak is a singlet.

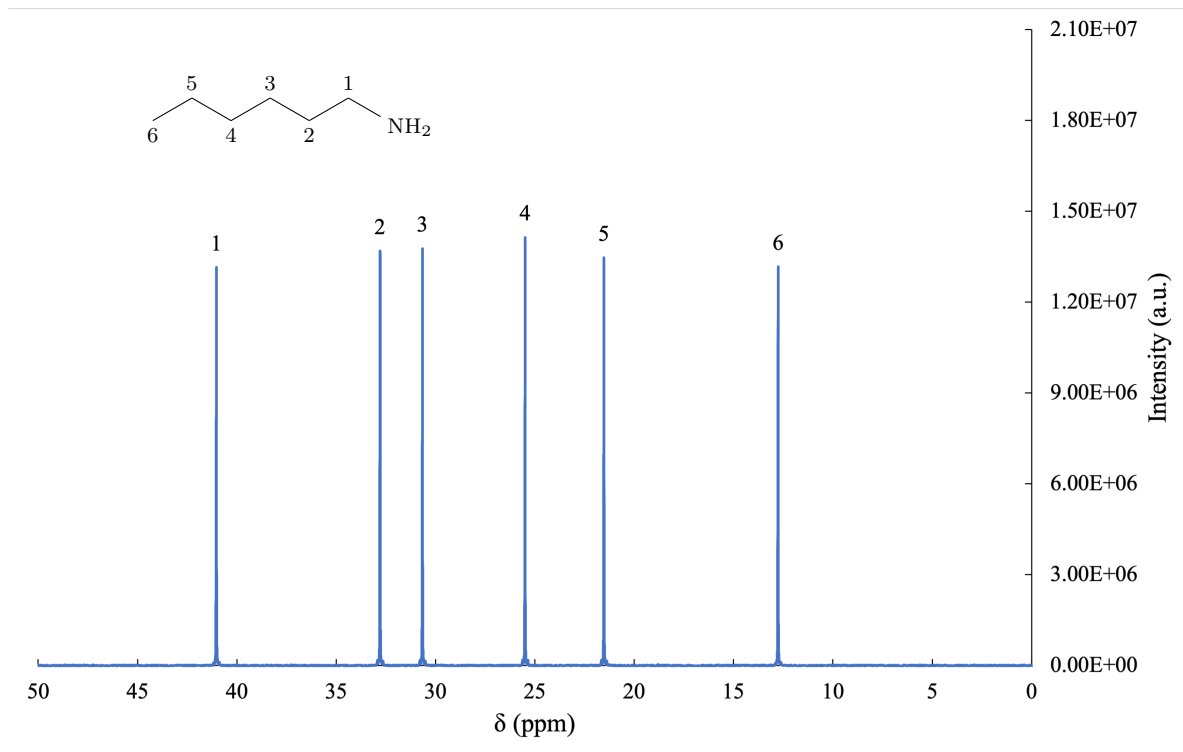


Figure 2:  $^{13}\text{C}$  NMR spectrum of hexylamine. Notice that carbon 1 is the most downshifted because it's closest to the electronegative nitrogen atom.

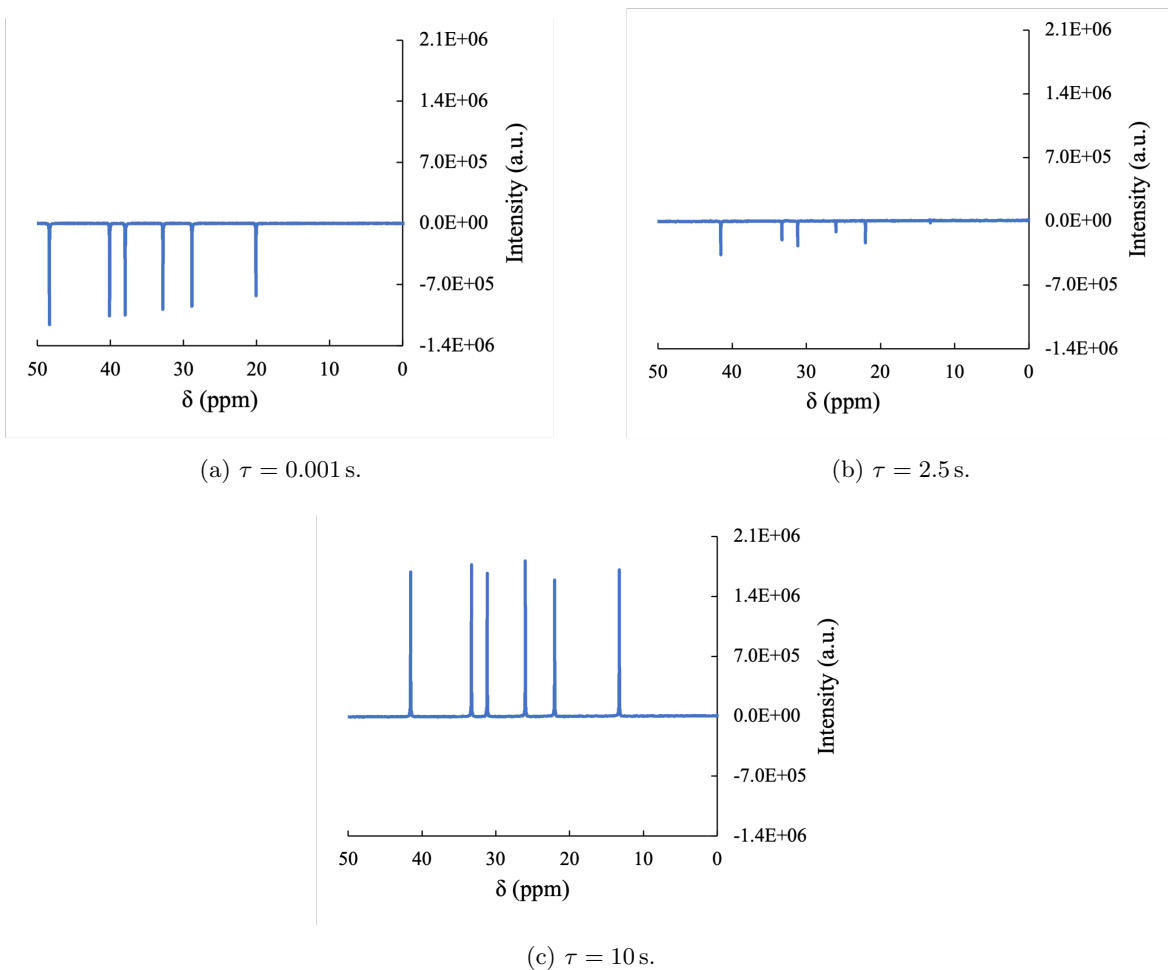


Figure 3: A selection of inversion recovery  $^{13}\text{C}$  NMR spectra for different delay times  $\tau$ .

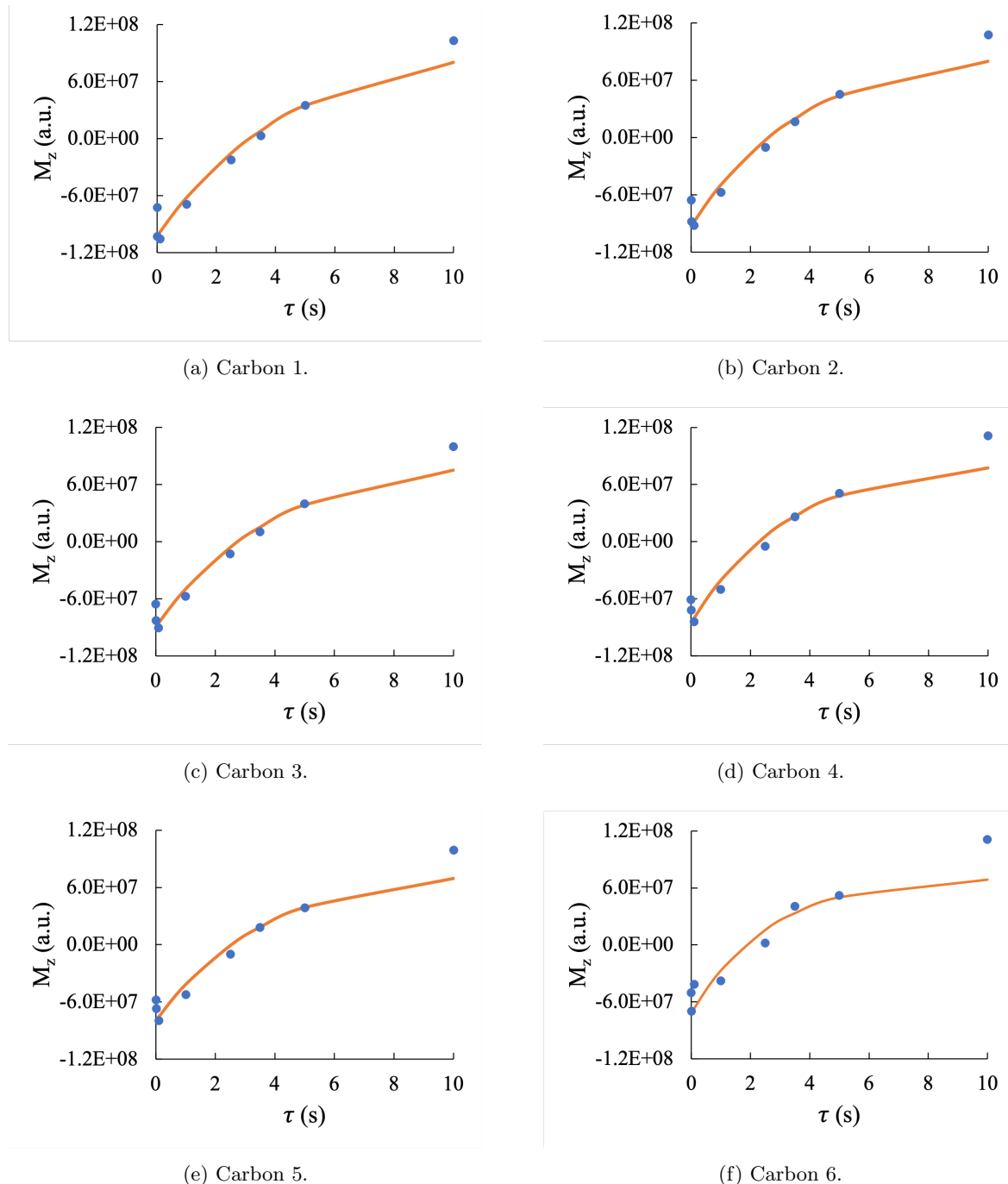


Figure 4: Determining the spin-lattice relaxation time  $T_1$  and the magnetization  $M_0$  at equilibrium via nonlinear regression.

Carbon 1	Carbon 2	Carbon 3	Carbon 4	Carbon 5	Carbon 6
15 197 494.17	15 490 978.25	14 146 608.68	17 608 862.89	15 739 108.37	21 625 158.79

Table 1: Standard errors for the above nonlinear regressions.

	Carbon 1	Carbon 2	Carbon 3	Carbon 4	Carbon 5	Carbon 6
$T_1$ (s)	4.52	3.75	3.99	3.29	3.67	2.66
$\tau_C$ (ps/rad)	5.15	6.21	5.83	7.07	6.34	5.83

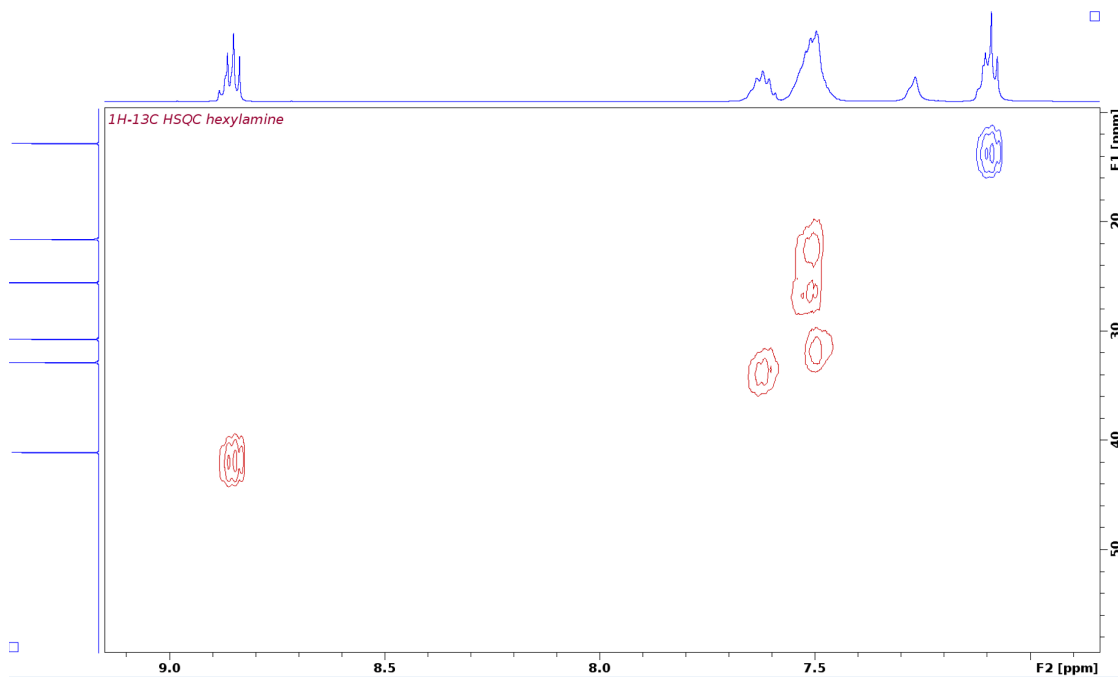
Table 2: The spin-lattice relaxation time and correlation time for each carbon in hexylamine.

Note that to calculate  $\tau_C$  from  $T_1$ , the formula

$$\frac{1}{T_1} = n \left( \frac{\mu_0}{4\pi} \right)^2 \frac{\hbar^2 \gamma_C^2 \gamma_H^2}{r_{CH}^6} \tau_C$$

was used, where the values of  $\gamma_C$  and  $\gamma_H$  were obtained from [bib:C13H1gyroempty citation](#) and the value of  $r_{CH}$  was obtained from [bib:CRCHandbookempty citation](#).

$T_1$  is the time constant governing how quickly magnetic spins return to equilibrium after a disturbance. The data in Table 2 shows that  $T_1$  trends downward for carbon atoms progressively farther from the amine moiety. This implies that carbons farther from the  $\text{NH}_2$  group return to equilibrium more quickly. This would support a theory that the hydrogen-bonding interactions present at the  $\text{NH}_2$  group restrict freedom in this molecule, and that portions of it farther from the center of restriction can move more freely and equilibrate more quickly. Since  $\tau_C$  is related to freedom of motion directly (it is literally a measure of the time required to change angle), the above commentary also applies to it.

Figure 5: Two-dimensional  $^1\text{H}$ - $^{13}\text{C}$  HSQC spectrum of hexylamine.

The peaks at the top of the HSQC spectrum in Figure 5 are analogous to those in the  $^1\text{H}$  spectrum of hexylamine. Similarly, those on the left side of the above image are analogous to those in the  $^{13}\text{C}$  spectrum of hexylamine. HSQC transfers magnetism between bound protons and  $^{13}\text{C}$  atoms atoms, so moieties that resonate in both forms of spectroscopy show up as two-dimensional peaks; in other words, each 2D peak corresponds to the proton above it and the carbon to the left of it. Thus, the six distinct peaks in the 2D spectrum correspond to the six carbons and their associated protons. The one hydrogen peak with no corresponding carbon peak represents the protons on the  $\text{NH}_2$  moiety, providing additional evidence for the identification of that peak beyond the fact that it's a singlet per rapid proton transfer-induced spin decoupling.

## References

- (1) Huber, K. P.; Herzberg, G. H. In *NIST Chemistry WebBook, NIST Standard Reference Database Number 69*, Linstrom, P. J., Mallard, W. G., Eds., <https://doi.org/10.18434/T4D303>; National Institute of Standards and Technology: Gaithersburg MD, 20899; Chapter Constants of Diatomic Molecules.
- (2) McNaught, I. J. The Electronic Spectrum of Iodine Revisited. *J. Chem. Educ.* **1980**, *57*, 101–105.
- (3) Lant, H. Electronic Spectroscopy: Absorption Spectra of Molecular Iodine in the Gas Phase, Rev. 1-21-23, 2023.
- (4) Verma, R. D. Ultraviolet Resonance Spectrum of the Iodine Molecule. *J. Chem. Phys.* **1960**, *32*, 738–749.
- (5) Saiz-Lopez, A.; Saunders, R. W.; Joseph, D. M.; Ashworth, S. H.; Plane, J. M. C. Absolute absorption cross-section and photolysis rate of I<sub>2</sub>. *Atmos. Chem. Phys.* **2004**, *4*, 1443–1450.

Steven Labalme  
9 February 2023

23 February 2023

## 5 GCMS ANALYSIS OF BENZENE IN GASOLINE

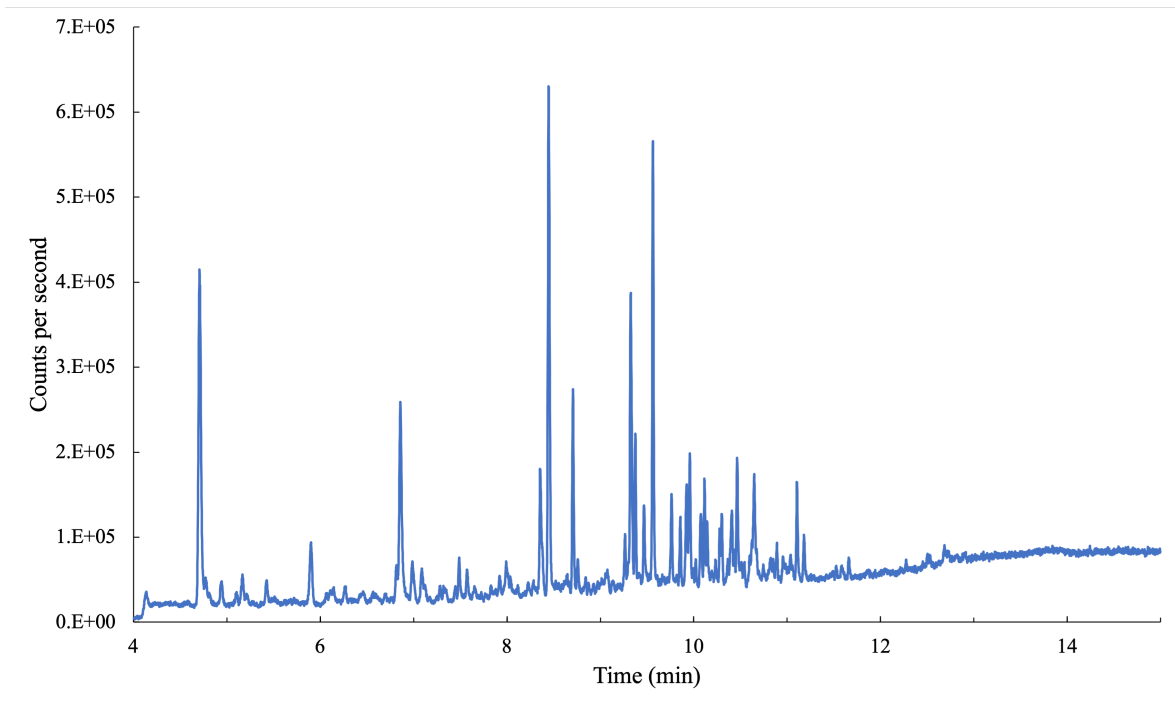


Figure 1: Total ion chromatogram of diluted 87-gasoline in pentane.

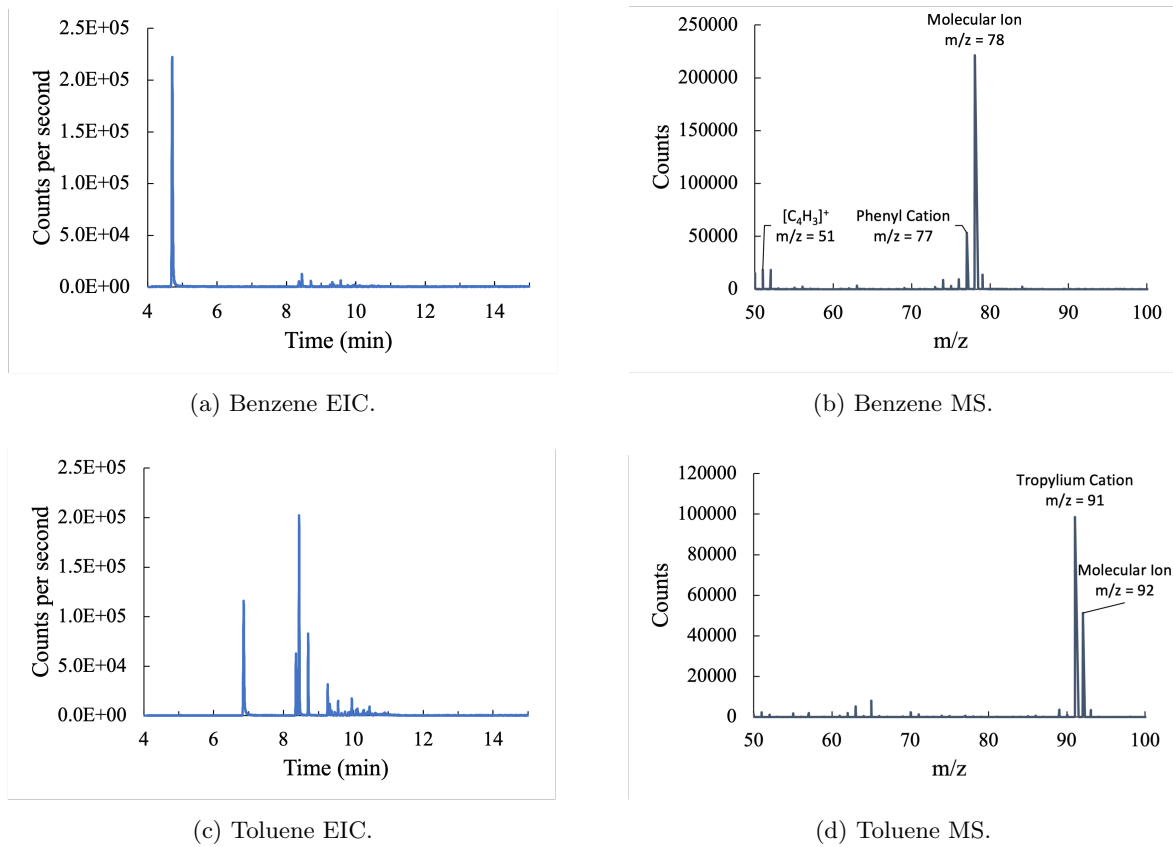


Figure 2: Extracted ion chromatograms and extracted mass spectra for benzene and toluene.

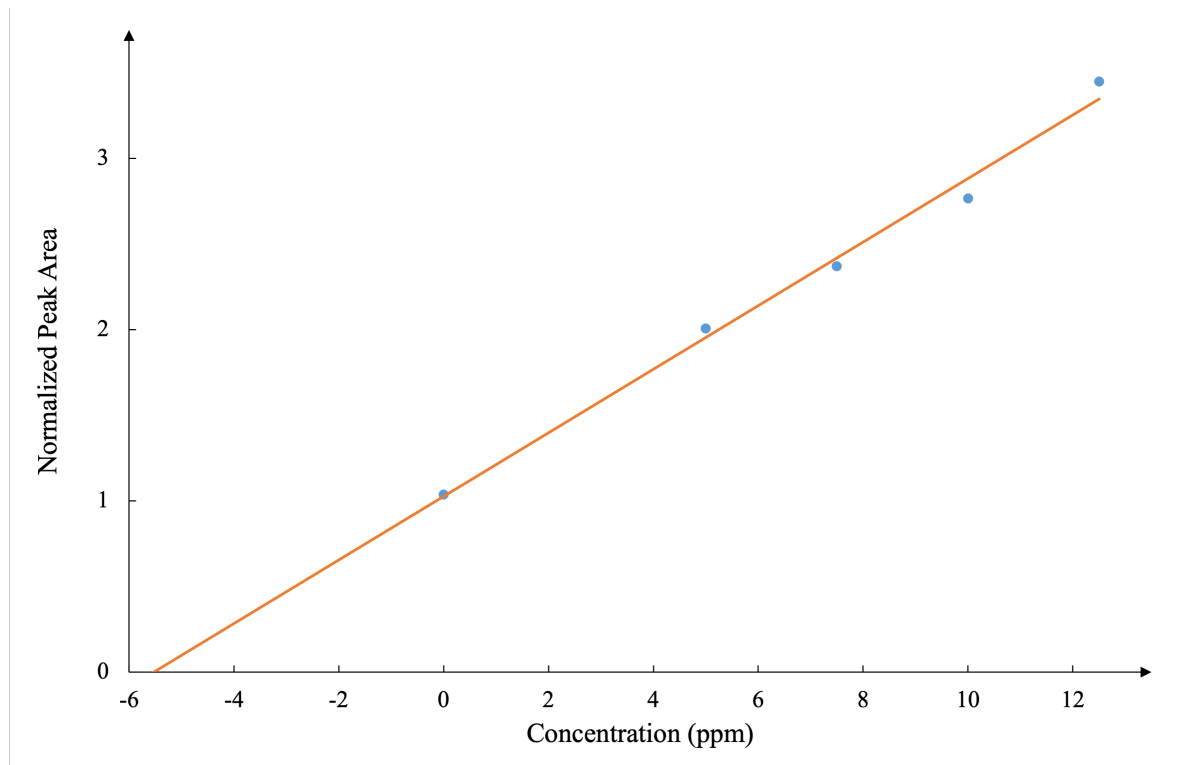


Figure 3: Standard addition of benzene.

Concentration (v/v)	Error (v/v)
$3.95 \times 10^{-4}$	$\pm 1.66 \times 10^{-4}$

Table 1: Concentration of benzene in gasoline.

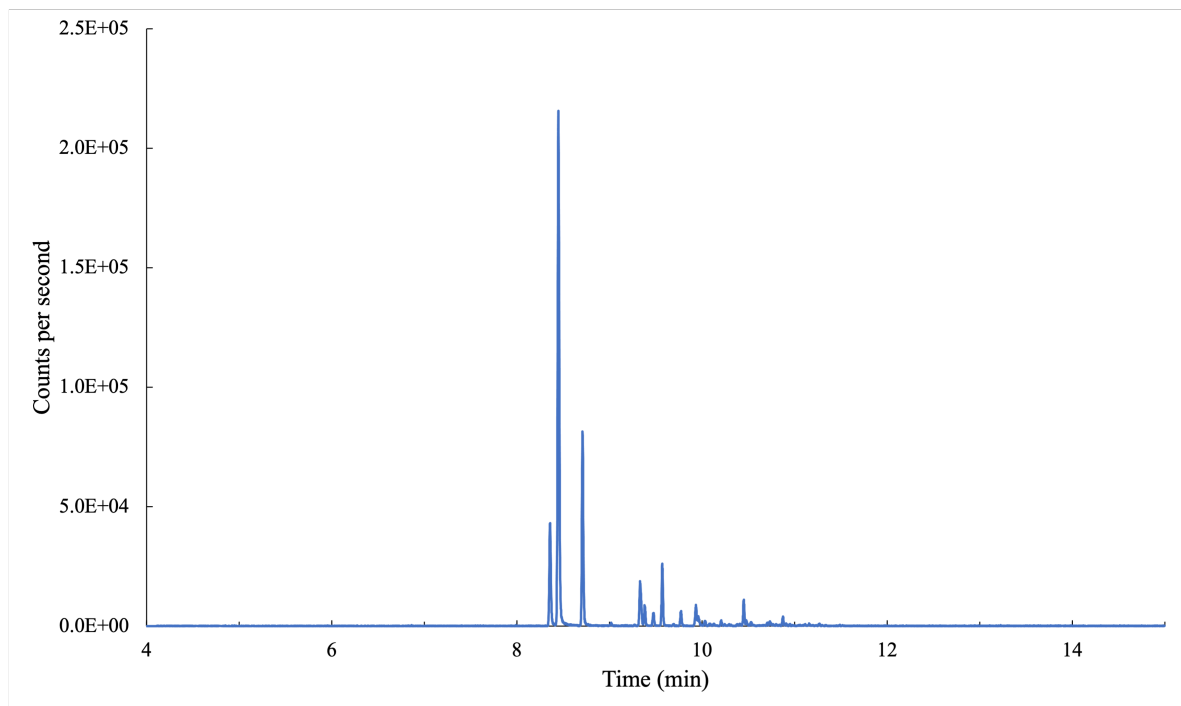


Figure 4: Extracted ion chromatogram of ethylbenzene.

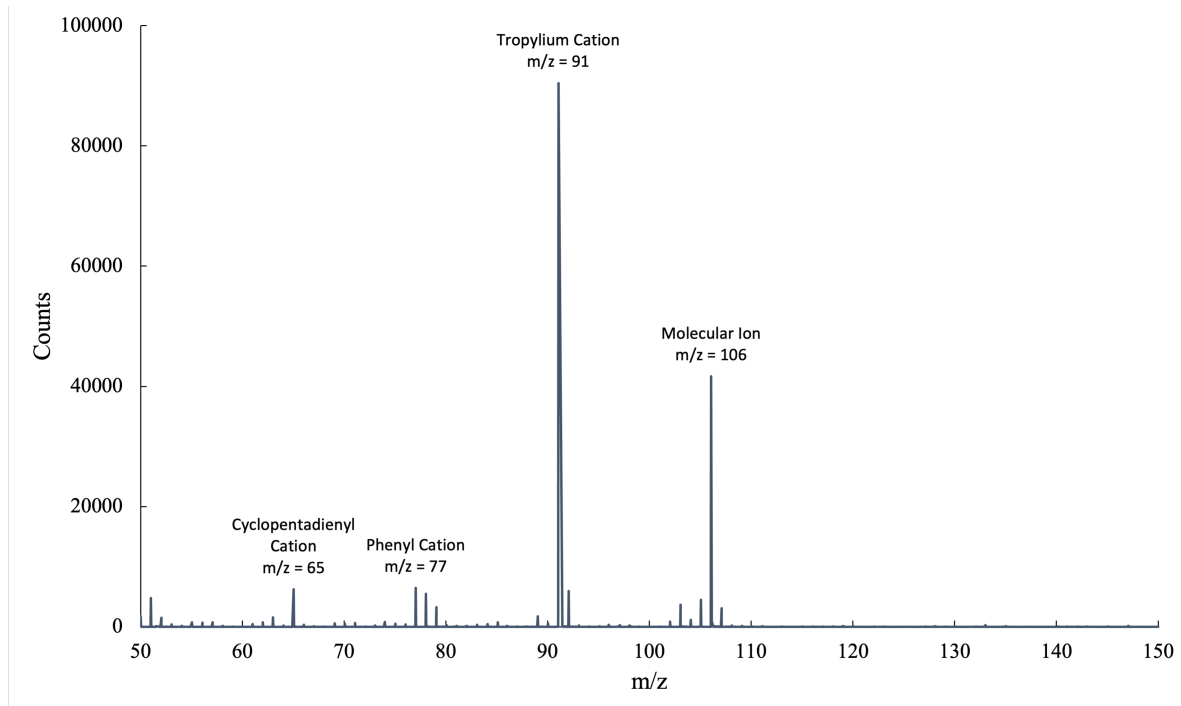


Figure 5: Extracted mass spectra of ethylbenzene.

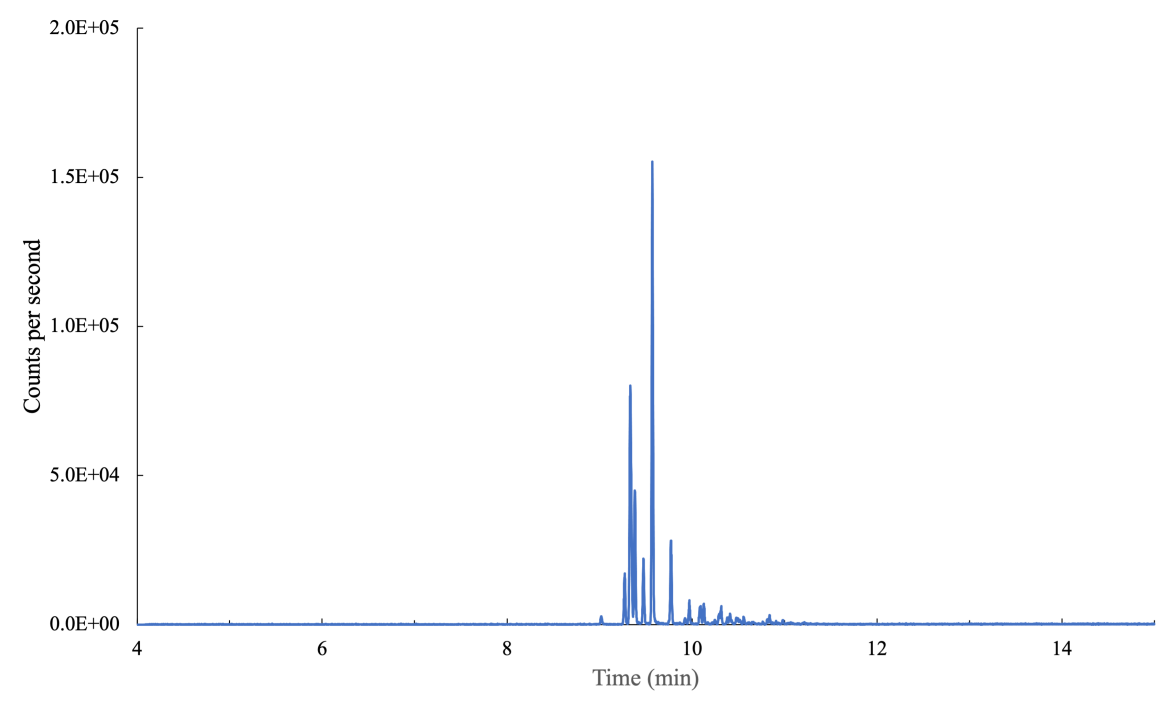


Figure 6: Extracted ion chromatogram of mesitylene.

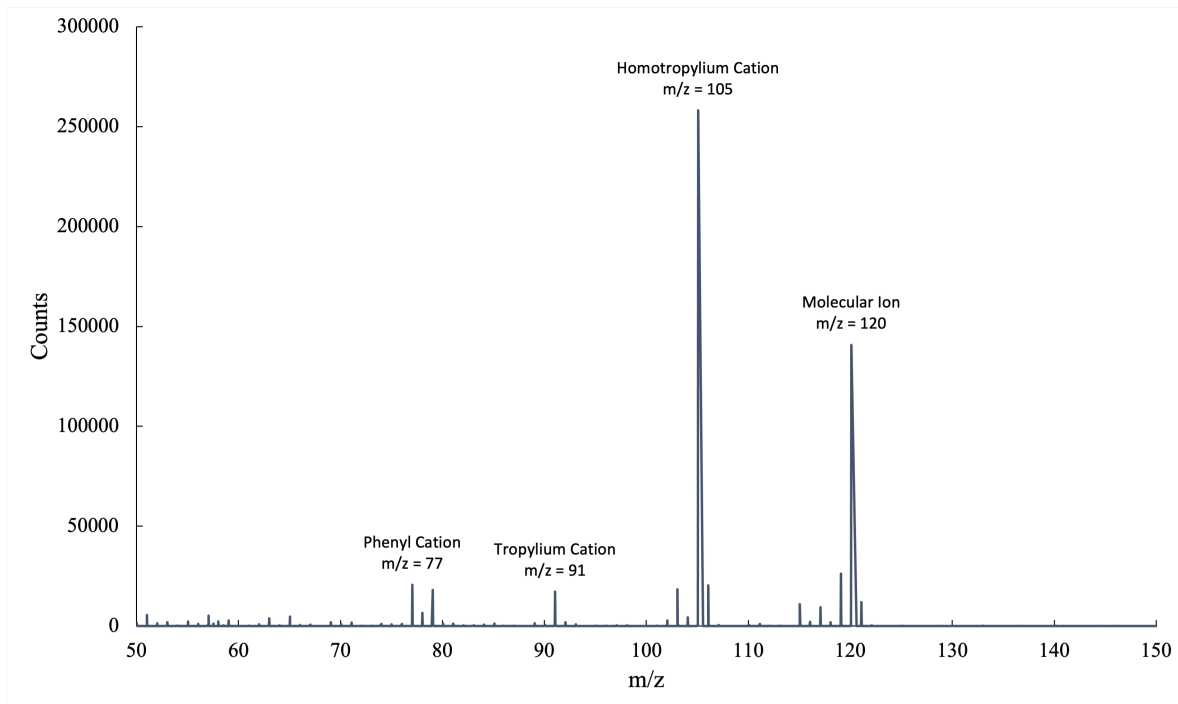


Figure 7: Extracted mass spectra of mesitylene.

	Ethylbenzene	Mesitylene
Concentration (ppm)	1.71	2.48

Table 2: Concentrations of additional aromatic molecules.

These substances may not follow the same peak area-to-concentration fit as benzene (Figure 3). Indeed, to more accurately determine the concentrations of these substances in gasoline, it would be appropriate to do a standard addition analysis for both of them, individually, instead of relying on more distantly related correspondences.